Superstructural Units in Lithium Borate Glasses

Nathan Barrow

Department of Physics, University of Warwick, Coventry, CV4 7AL

March 2006

Abstract

Ten glasses of nominal composition $x Li_2O \cdot (100-x) B_2O_3$ were prepared over the range x = 0 to 40 mol%. A boron-11 NMR investigation has provided the fraction of 4-coordinated boron in the samples and this is consistent with previous studies. Raman spectra showed the intermediate range order associated with this type of binary borate glass. Six glasses of nominal composition $x CoO \cdot (20-x) Li_2O \cdot 80 B_2O_3$ were prepared over the range x = 0.1 to 5 mol%. It is shown that accurate determination of N4 fraction in glasses from boron-11 NMR spectra is unattainable for samples having a magnetic (mass) susceptibility approximately greater than 2 $m^3 g^{-1}$, which corresponds to 2 mol% cobalt oxide.

I. Introduction

Borate glasses have been well studied over the past decade and there has been much research into their structure and spectra. This interest is partly because of the anomalous behaviour of the glass in that it forms superstructural units: well defined arrangements of the basic BO_3 and BO_4 structures (Fig. 1) [1]. ~~See figure 1.~~ BO_3 forms a planar triangle whereas BO_4 has a tetrahedral arrangement of oxygen around the boron atom.

Borates are used in the formation of borosilicate glasses that are used to immobilise high level nuclear waste for long term storage. The existence of superstructural units in these glasses could have important consequences on the final structure of the nuclear waste glass, so it is worthwhile investigating the superstructure of simpler binary borate glasses.

Evidence for the existence of these superstructures in B_2O_3, which do not occur in other glasses, is the sharp line witnessed in Raman spectra corresponding to the breathing mode of the boroxol group [2,3].

Pure B_2O_3 forms a glass by itself and forms binary borates with many oxides. While pure B_2O_3 only consists of 3-coordinated 'B3' boron at standard pressure, the addition of cations makes 'B4' boron structures possible. This is basically because it is more energetically favourable to form BO_4 tetrahedra than break B-O-B bridges and leave a non-bridging oxygen. This is discussed in detail by Wright, Vedishcheva and Shakhmatkin [1]. This special behaviour gives borate glasses the ability to form superstructural units, some of which are shown in figure 1.

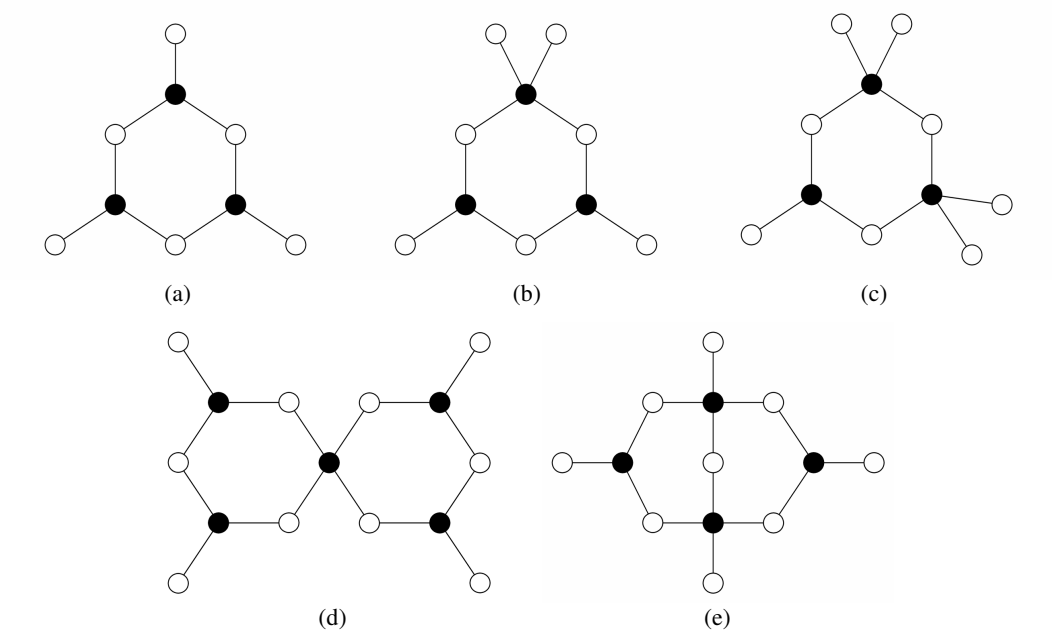

Figure 1. A selection of superstructural units composing of boron (●) and bridging oxygens (○)
(a) boroxol ring, B_3O_6; (b) triborate, B_3O_7; (c) di-triborate, B_3O_8; (d) pentaborate, B_5O_{10}; (e) diborate, B_4O_9

An interesting parameter of borate glasses is the N4 fraction, which is the amount of 4-coordinated boron compared to the total amount of boron:

$$N4=\frac{B4}{B3+B4} \tag{1}$$

Hence, pure B_2O_3 has an N4 fraction of zero and a hypothetical borate glass consisting of nothing but diborate units would have an N4 fraction of 50%. The proportion of 4-coordinated boron is detectable by, amongst other means, Raman spectroscopy and NMR spectroscopy. The most extensive study on lithium borates was performed by Jellison, Feller and Bray in 1978 [4]. They showed the N4 fraction peaking at around 40 mol% Li_2O with a proportion of approximately 0.45 B4 to 0.55 B3.

A primary aim of this project is to correlate the N4 fraction given by NMR spectroscopy to that given by Raman spectroscopy. This is worthwhile as various radioactive elements that would be present in the nuclear waste glass, such as uranium and its oxides, are paramagnetic, which prevents NMR spectroscopy being performed when these species are in high abundance. However, Raman spectroscopy does not depend on the magnetic susceptibility of the sample. By correlating the two techniques the N4 fraction can be found from the Raman spectrum of a glass containing too much paramagnetism to be analysed with NMR. Although Raman scattering produces a spectrum unaffected by magnetisation of the sample, the spectrum is significantly harder to interpret in terms of N4 fraction than an NMR spectrum.

One of the seminal papers in the field of Raman spectroscopy of borate glasses is by Konijnendijk and Stevels (1975), and offers insight into which peaks correspond to which superstructural units in borate glasses [5]. Another key study into superstructural unit peak assignment was performed by Kamitsos, Karakassides and Chryssikos (1989), in which they concentrated on caesium, rubidium and potassium

binary borates [6]. Meera and Ramakrishna also contributed to the peak assignment debate in 1991 discussing a wide range of borate glasses [2].

Densities and structural models for various alkali borates, including lithium and caesium, were investigated by Royle et al [7]. Neutron diffraction studies of caesium borate glasses performed by Shaw et al. have provided further information about the role of superstructural units in vitreous B_2O_3 and borate glasses [8]. Massot, Souto and Balkanski have tested borate glasses with Raman and light scattering spectroscopy as well as acoustic wave velocity and glass density measurements to help describe the short and medium range order [9].

NMR spectroscopy is very useful in the study of borate glasses as it can clearly distinguish between the two chemically distinct B~~N~~3 and B~~N~~4 sites and quantify the proportion of each. In 1993 Wüllen and Müller-Warmuth showed that MAS-NMR was a reliable method to do this in both theory and experiment [10]. However, as boron-11 is a quadrupolar species, this single-quantum method contained second order anisotropies. Amoureux, Fernandez and Frydman showed how to optimise an earlier multiple quantum experiment on half-integer quadrupoles [11]. This led to a study of the short range order in B_2O_3 by Hwang et al [12]. A helpful communication on the theory of MQMAS containing further optimisation methods is provided by Brown and Wimperis [13].

Using 3QMAS-NMR Stebbins, Zhao and Kroeker have directly measured the concentrations of non-bridging oxygens in borate glasses [14]. Kroeker has also related the B~~N~~4 sites in caesium borate glasses to superstructural units using MAS-NMR [15]. The proportion of B~~N~~4 in the borate glass as alkali modifier content is varied has been explored, again using MAS-NMR, by Clarida et al [16]. Du and Stebbins have examined, using 3QMAS-NMR, the connectivities within borate glasses and shown that there are boroxol rings [17]. Further studies on the NMR response of boroxol rings were performed by Zwanziger in 2004 [18].

II.1 Glass Forming Theory

Glasses have no long range order and are thermodynamically unstable compared to crystals, having a higher enthalpy for a given temperature. Glasses also exhibit time-dependeant behaviour during formation; their final enthalpy will depend on their rate of cooling, which is not the case for crystals. On cooling a liquid below its melting point it can suddenly order itself causing a sharp drop in enthalpy, or it can remain disordered and become a supercooled liquid. As temperature continues to drop the viscosity of the liquid will rise until the rearrangement of atoms ceases, leaving a disordered solid. This explains the time-dependence, as faster cooling will leave less time for atomic rearrangements to lower enthalpy.

Vitreous B_2O_3 forms a glass on cooling, contains only B3 and is thought to comprise ~~of~~ locally independent interpenetrating networks made up of boroxol groups and BO_3 triangles, as opposed to one large single network. Introducing cations initially (upto 40 mol%) converts BO_3 triangles into BO_4 tetrahedra. This increase in coordination number strengthens the network [1].

The addition of 4-coordinated boron in the network allows the possibility of having different superstructural units to the boroxol group. One determination of the fractions of superstructural units present as a function of composition is shown in figure 2:

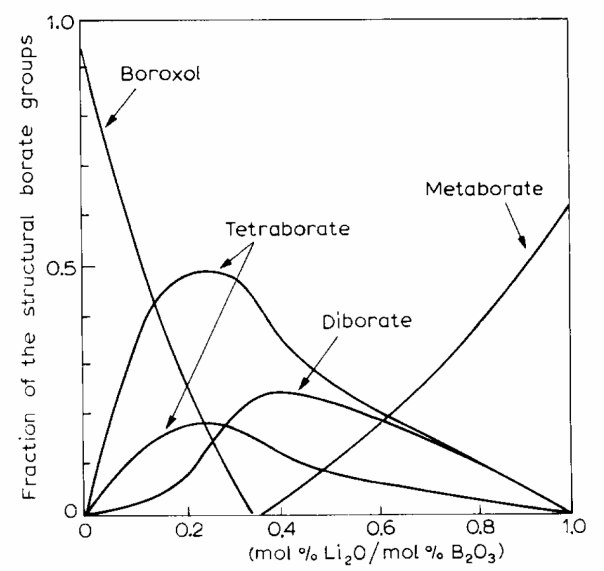

Figure 2. The intensities of Raman signals of boroxol rings, tetraborate and diborate configurations as a function of mol% Li_2O/mol% B_2O_3 [19]

Meera and Ramakrishna have a differing view for the structural groups present at various compositions of xLi$_2$O·(100-x)B$_2$O$_3$, mainly by the inclusion of pentaborate and dipentaborate and the exclusion of tetraborate [2]. Tetraborate can be considered to be pentaborate and triborate joined by a bridging oxygen and so not a true superstructural unit.

II.2 Nuclear Magnetic Resonance Spectroscopy Theory

NMR is used as a probe of local structure in materials. It is a technique particularly suited to glasses as their lack of long-range order prevents their structure from being determined easily by X-ray diffraction, as is the case for crystals. NMR works because in a magnetic field every particle has a magnetic moment, μ, and this is proportional to the intrinsic spin of the particle by the gyromagnetic ratio, γ. Just as a compass needle with a magnetic moment rotates in the presence of a magnetic field, so does a nuclear spin. But unlike a compass needle that aligns itself to minimise the magnetic potential energy, a nuclear spin precesses around the magnetic field lines, always keeping at the same angle.

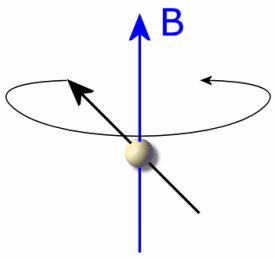

Figure 3. Spin precession of a magnetic moment in a magnetic field, B.

The frequency of this precession is proportional to the strength of the magnetic field, B_0, and the gyromagnetic ratio:

$$\omega_0 = -\gamma B_0 \quad (2)$$

Different nuclei possess different gyromagnetic ratios and will precess at different frequencies in the same magnetic field. This allows NMR spectroscopy to be a nucleus~~i~~-specific technique. Even if the magnetic field is perfectly homogenous on a macroscopic level, there will be small deviations caused by the presence of atoms and molecules, as electrons are magnetic and distort the field. This effect is called chemical shift because, as there will be different local-magnetic-field strengths around chemically distinct nuclei, the precessional frequency (given in equation 2) will be slightly different. As B3 and B4 boron-11 are in different chemical (and hence magnetic) environments their spins will precess at slightly different frequencies and so the separation of the two sites will be easily determined by using NMR.

Although it has been said that nuclear spins do not change their angle of precession in a magnetic field, there is a small effect caused by thermal vibrations, such that over millions of precessions an ensemble of nuclear spins generate a small net magnetic moment aligned with the applied magnetic field. This is the microscopic mechanism for nuclear paramagnetism, and is about four orders of magnitude weaker than electron diamagnetism. As such the net magnetic moment of the nuclear spins cannot be detected directly.

The method of detection used in NMR is to bombard the sample with electromagnetic radiation. It is the magnetic part of the wave that interacts with the nuclear magnetic moments and, as shown in equation 2, the spins will precess around the magnetic field of the wave. This oscillating magnetic field is weaker than the static field and the frequency of the pulse is tuned to 'resonate' with the nuclear spin to have an effect. This is a similar situation to~~of~~ sound being able to shatter glass; only the correct pitch will have an effect. The frequency in the case of nuclear spins falls in the radio region.

For a fixed power the duration of the RF (radio-frequency) pulse governs by what angle the individual spins, and in turn the net magnetic moment, will be rotated ~~by~~. The pulse can be applied to flip the spins by 90°. Once the pulse is gone, microscopically, the spins carry on precessing around the static magnetic field, as before. But macroscopically, instead of being aligned with the magnetic field, the net magnet moment starts precessing around as well, perpendicular to the magnetic field in this 90° case. This rotating magnetic moment generates a rotating magnetic field, and a changing magnetic field generates an electric field, according to Maxwell's equations. This tiny, oscillating, electric field is picked up by a coil of wire, amplified and sent to a computer.

Over time, the same action that causes a slight bias in the magnetic alignment of the spins causes the spins to line up with the main magnetic field once again. This is called spin-lattice relaxation. Additionally, the individual spins can fall out of synchronisation with each other due to the inhomogeneous magnet fields present across the sample. This causes the net magnetic moment to decrease in magnitude and is called transverse relaxation.

Archaically, the term 'spin' was used because the mathematics involved with the phenomenon looked similar to classical angular momentum; the term does not reflect

the actual physical rotation of a particle. Many particles have half-integer spin, a value not allowed classically. The quantum numbers governing the angular momentum energy eigenstates are I (which can have any positive integer or half-integer value) and M (which has values from –I to +I in integer steps). For quantum number I = 3/2, M can have any of the following values; -3/2, -1/2, +1/2, +3/2, as shown in figure 4:

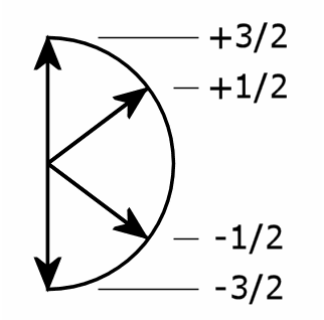

Figure 4. The four energy states allowed for a particle with spin I = 3/2.

Boron-11 has a nuclear spin of 3/2 and has both electric dipole and electric quadrupole moments. The quadrupolar moment of the nucleus, Q, interacts with the electric field gradient, which can be defined by a second-rank symmetrical tensor, V:

$$V = \begin{pmatrix} V_{xx} & 0 & 0 \\ 0 & V_{yy} & 0 \\ 0 & 0 & V_{zz} \end{pmatrix} \tag{3}$$

The diagonal components represent~~ing~~ the electric field gradient in the *x*, *y*, and *z* directions respectively. From this, two parameters can be defined; *eq*, which is related to the quadrupole linewidth and η, which is the asymmetry parameter:

$$eq = V_{zz} \tag{4}$$

$$\eta = \frac{V_{xx} - V_{yy}}{V_{zz}} \tag{5}$$

The strength of the quadrupolar coupling constant, *Cq*, is then:

$$Cq = \frac{e^2 qQ}{\hbar} \tag{6}$$

The dipole moments, which cause first-order broadening of the spectral lines, can be removed by spinning the sample at a so-called 'magic' angle of 54.7° to the magnetic field. The quadrupole moments cause second-order broadening by interacting with the electric field gradient in the sample. This broadening can be removed by spinning the sample at 30.6° or 70.1°, but this would cause the first-order broadening to reappear. Thus second-order 'quadrupolar' broadening can only be partially removed by rotation around a single axis. The angles given here are the roots of the Wigner rotation matrices for second rank (54.7°) and fourth rank (30.6° or 70.1°) cases and are further discussed by Llor and Virlet [20].

Double rotation experiments (DOR) can remove this second-order quadrupolar broadening, but the technique is complicated and limited to slow rotation speeds.

Triple-quantum magic angle spinning (3QMAS) is an experiment that separates the overlapping spectral lines by producing a 2D spectrum [11-14]. Although the second-order broadening is still present in the direct dimension, taking a projection along a diagonal shows the unbroadened quadrupole lines corresponding to the different chemical environments of B3 and B4 boron.

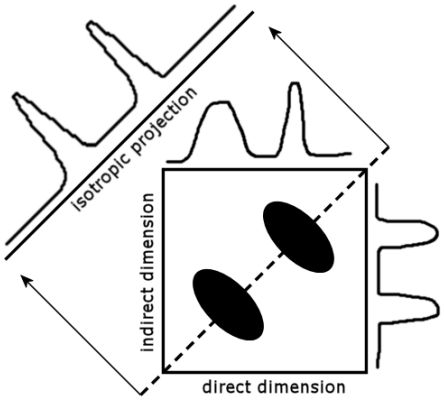

Figure 5. A schematic of how MQMAS can remove second-order broadening by taking an isotropic projection.

At high enough magnetic fields to reduce the quadrupolar broadening, a one-pulse MAS experiment is suitable for distinguishing between B3 and B4 as the different species are in different magnetic environments and will show different chemical shifts. This experiment will provide two peaks and by comparing the integral under each of the two curves the proportion of B4 to B3 can be found. Theory predicts there are actually two separate, overlapping lines under each peak. For example, the one pulse spectrum of pure B_2O_3 shows one broad line that is really two overlapping lines corresponding to the different environments of boron in the structure, that is, symmetric and ~~anti~~symmetric [22].

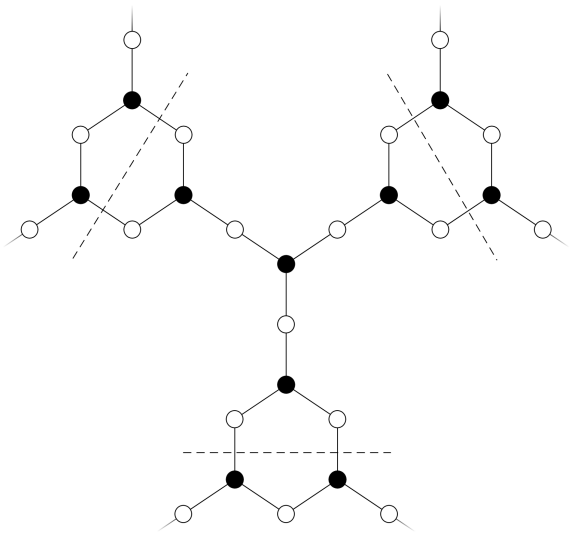

Figure 6. A schematic diagram showing how boron (●) and bridging oxygens (○) make up boroxol groups and BO_3 triangles. The dashed lines enclose the repeated unit. The central boron is in a symmetric environment, whereas the borons in the boroxol groups are in a~~nti~~symmetric environments.

To deconvolute the two lines under the curve a phase modulated split-t1 triple-quantum MAS experiment can be used; see figure 6. This pulse sequence excites the triple-quantum coherence of the boron nucleus [13].

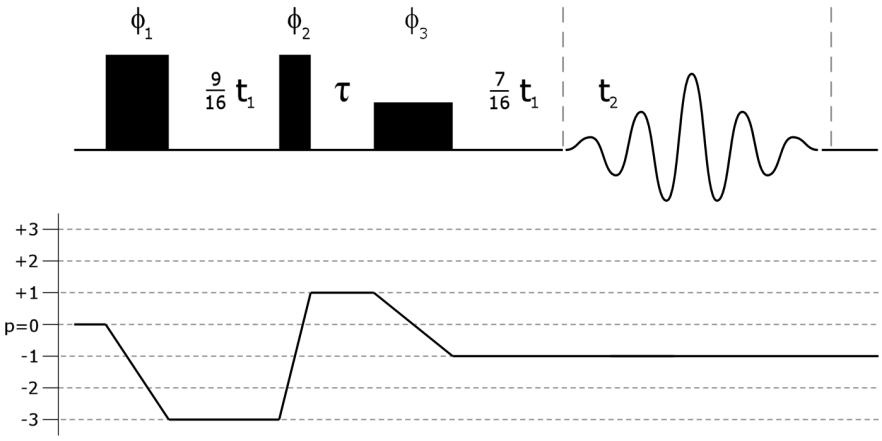

Figure 6. The pulse sequence and coherence pathway for the phase modulated split-t1 3QMAS experiment.

The first two pulses in figure 4 are 'hard': they excite all the transitions of the spin 3/2 nucleus $\left(+\frac{3}{2} \leftrightarrow +\frac{1}{2},\ +\frac{1}{2} \leftrightarrow -\frac{1}{2},\ -\frac{1}{2} \leftrightarrow -\frac{3}{2}\right)$. The first pulse length is optimised to give the largest triple quantum coherence amplitude and the second pulse length is optimised to provide the maximum conversion from the -3 to the +1 coherence. The third and final pulse is 'soft' and so just excites the central transition $\left(+\frac{1}{2} \leftrightarrow -\frac{1}{2}\right)$ to put the coherence in the -1 pathway ready for quadrature detection at time t_2.

The experiment is called 'split-t1' as the t_1 period is shared between the triple quantum evolution and single quantum evolution, as shown by the coherence pathway in figure 6. This causes the second order quadrupolar broadening to become refocused at the end of the t_1 period, which not only removes the need for double angle rotation but also avoids the need for additional processing (shearing) that similar pulse sequences have to undergo. This pulse sequence acquires a whole echo and is programmed such that it appears at a fixed position in t_2 [13].

II.3 Raman Spectroscopy Theory

When intense, monochromatic, light is incident on a material most of the photons are elastically scattered (Rayleigh scattering) and so have the same energy as the incident photons. The Raman spectrometer filters these photons out with a holographic filter, leaving only those photons that have scattered inelastically (Raman scattering) to reach the detector. Raman scattering occurs when there is a change in the energy of the molecule, in this case; vibrational energy.

The incident photon interacts with the electric dipole of the molecule, which excites the molecule's energy into a virtual energy state. De-excitation occurs in less than 10^{-14} seconds with the emission of a photon. If the final energy is greater than then the initial energy then the process is called 'Stokes' Raman scattering, which leaves the

photon with less energy than it started with. This is what is observed in Raman spectroscopy [21].

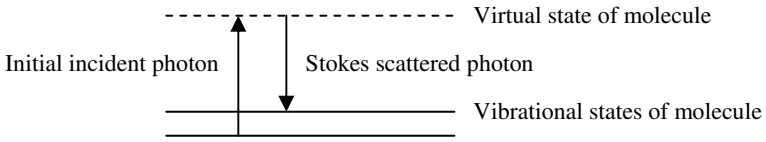

Figure 7. An energy level diagram for Raman scattering. The photon gives up some of its energy in exciting the vibrational ground state of a molecule.

A spectrum is created by plotting the intensity of Raman scattered photons as a function of wavenumber, ν.

$$\nu = \frac{1}{\lambda_{incident}} - \frac{1}{\lambda_{scattered}} \tag{7}$$

Where $\lambda_{incident}$ is the wavelength (in cm) of the incident laser photons and $\lambda_{scattered}$ is the wavelength (in cm) of the detected scattered photons.

Different structural units (see figure 1) will have different vibrational modes. At room temperature the strongest vibrational mode in borate glasses is the lowest energy 'breathing' mode of the boroxol unit. By acquiring a spectrum of these modes it is possible to match up peaks corresponding to various structural units. Combining the peak areas and N4 fraction for each structural unit it is possible to find the total fraction of N4 as a function of glass composition.

The boroxol group is known to peak around 806 cm^{-1}, six-membered rings some amount of 4-coordinated boron peak around 770 cm^{-1}, and the diborate group peaks around 1150 cm^{-1} [5].

III.1 Glass Creation Details

The balanced stoichiometric equation for creating lithium borate is:

$$Li_2CO_3 + B_2O_3 \xrightarrow{\text{heating}} Li_2O \bullet B_2O_3 + CO_2$$

Whether the product is crystalline or vitreous depends on the cooling rate of the melt. In this investigation ten glasses were made of various nominal compositions to give a product $x Li_2O \bullet (100-x) B_2O_3$ over the range x=0 to x=40. The paramagnetic compound iron oxide (Fe_2O_3) was added at a concentration of 0.1 molar percent to each composition to de~~in~~crease the spin-lattice (T_1) relaxation time of the nuclear spins and hence speed up the NMR acquisition process.

x	Li_2CO_3 (g)	B_2O_3 (g)	Fe_2O_3 (g)
0	0.000	20.000	0.046
5	1.093	19.558	0.047
10	2.251	19.090	0.049
15	3.482	18.592	0.050
20	4.792	18.062	0.052
25	6.190	17.497	0.054
30	7.684	16.893	0.055
33 1/3	8.738	16.466	0.057
35	9.284	16.246	0.057
40	11.003	15.550	0.059

Table 1. Mass measurements to make 20 grams of nominal composition of $x Li_2O \bullet (100-x) B_2O_3$.

All compositions were weighed out on the same calibrated Oertling balance to 3 decimal place accuracy. The pre-melt powders were put in glass jars and shaken well to roughly homogenise the different reactants before being stored in a desiccator. Due to the iron oxide, the lower the lithium carbonate content the pinker the mixed powders appeared.

Two compositions were fired in an electrically heated furnace at the same time in large platinum-rhodium crucibles (with mass around 250g). The large crucibles were necessary to prevent the overflow of material due to gas evolution on heating. The furnace was programmed to ramp at 10°C a minute before dwelling at 1000°C. When the furnace reached this temperature a stopwatch was started and after 20 minutes the melts were poured from their crucibles onto a graphite coated steel plate that was at 200°C. The hotplate was then turned off and left to cool naturally. This procedure is designated method 1. See figure 8:

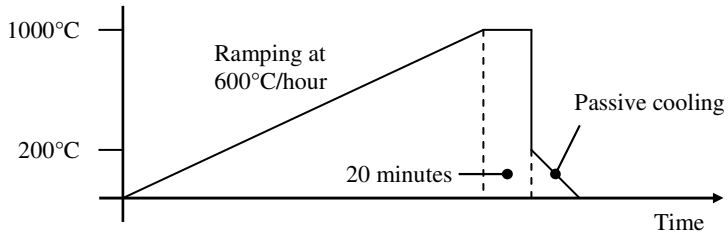

Figure 8. The heating program for method 1 lithium borate glass creation (not to scale).

The nominal compositions were reweighed as in table 1 and the above process repeated exactly, except instead of the graphite coated steel plate being at room temperature, the melt was plate quenched to rapidly cool it to form a glass. This new method has the advantage of forming thin sheets of glass that are easier to grind up for analysis and is designated method 2.

A third reweighing and firing with a halved ramping rate of 5°C a minute was performed for reweighed nominal compositions of x=35 and x=40. This is method 3.

In addition to the binary borate glasses, six samples containing cobalt oxide substituted~~tracted~~ for di-lithium oxide were also prepared. All six had the boron oxide proportion fixed at 80 mol%. As cobalt oxide is paramagnetic there was no need to add iron oxide. Method 3 was employed for the creation of these samples.

x	$CoCO_3$ (g)	Li_2CO_3 (g)	B_2O_3 (g)
0.1	0.039	4.765	18.049
0.2	0.077	4.738	18.036
0.5	0.192	4.656	17.996
1	0.383	4.520	17.931
2	0.760	4.251	17.802
5	1.861	3.468	17.425

Table 2. Mass measurements to make 20 grams of nominal composition of xCoO• (20-x)Li_2O•80B_2O_3.

III.2 NMR Experimental Details

Boron has two isotopes, boron-10 and boron-11. Boron-11 will be probed as it is 80% naturally abundant and has a nuclear spin of 3/2. Boron-11 has gyromagnetic ratio of 8.585×10^7 rad T^{-1} s^{-1}, roughly a third that of the proton. The spectrometer used was a Varian Chemagnetics CMX 600 (14.1 T) spectrometer operating at 192.5 MHz. The well ground samples were packed in 4 mm diameter zirconia rotors and spun at 10 kHz in a CMX 4mm probe (serial #6300). Boron phosphate (BPO_4) was used as a secondary reference, having a single spike at -3.3 ppm, with respect to the primary reference Et_2O:BF_3 at 0 ppm.

A pulse-delay array experiment was run on the (arbitrarily chosen) x=40 sample to determine the most suitable time delay between pulses. Due to the iron oxide, spin-lattice relaxation was very quick and it was determined that 0.1 seconds between pulses was enough time to allow the bulk nuclear magnetisation to realign with the static magnetic field. A pulse-length array experiment was also run, giving the π-flip

angle to be 10.5 µs, which makes the nutation frequency for this particular probe's power 300 k~~K~~Hz, giving B_{RF} = 1.56 mT. –surely not? Too high?

All the samples from *x*=0 to *x*=40 were then recorded using an identical experimental procedure. The pulse sequence was just one 0.60 µs pulse at 192.547 MHz, phase cycled over four acquisitions to remove the quadrature ghost that appears at the pulse frequency (192.547 MHz) in the spectra. After the pulse there was a 2.5 µs receiver delay and then a 2.5 µs acquisition delay to allow the 'ringing' in the coil to dissipate as well as give time for the measurement electronics to recover. Then followed 4096 measurements, 2.5 µs apart, giving a total acquisition length of 10.24 ms. This experiment was repeated 2048 times to improve the signal-to-noise ratio.

The phase modulated split-t1 triple-quantum MAS experiment, shown in figure 6, ~~required more setting up~~s experimentally more complex than the one-pulse experiment. The *x*=0 sample was tested first as it has the least complicated spectrum. To begin, each of the three pulse lengths were varied separately to discover the optimum pulse length for each one. The following lengths; excitation pulse – 6 µs, conversion pulse – 2.3 µs, echo pulse – 11.2 µs, were determined to give the best signal-to-noise ratio. The pulse sequence makes use of phase cycling to select the appropriate coherence pathway, so the signal is added over multiples of 96 acquisitions. Adding the signal from 4608 acquisitions produced an acceptable signal-to-noise ratio. The pulse lengths were later changed to the following; excitation pulse – 8 µs, conversion pulse – 3.25 µs, echo pulse – 12.5 µs, which yielded slightly improved signal-to-noise for the *x*=20 sample.

The data acquired in the 1D experiment, a free induction decay (FID) signal, was processed in Spinsight. The FID had one extra initial point back-predicted to make up for the acquisition delay and thus reduce the need for first-order phasing. The FID then underwent a complex fast Fourier transform to convert the time signal into the frequency domain. The spectrum was then zero-order phased so that the 'real' part was purely 'absorptive', that is, all positive. A DC-offset was finally applied to put the lineshape down on the baseline and prevent spurious peak fits.

Peak fitting was performed using a program called DMFit [23]. The B3 peak was fitted with two quadrupole lineshapes and the B4 was fitted with two 50% Gaussian-50% Lorentzian lineshapes.

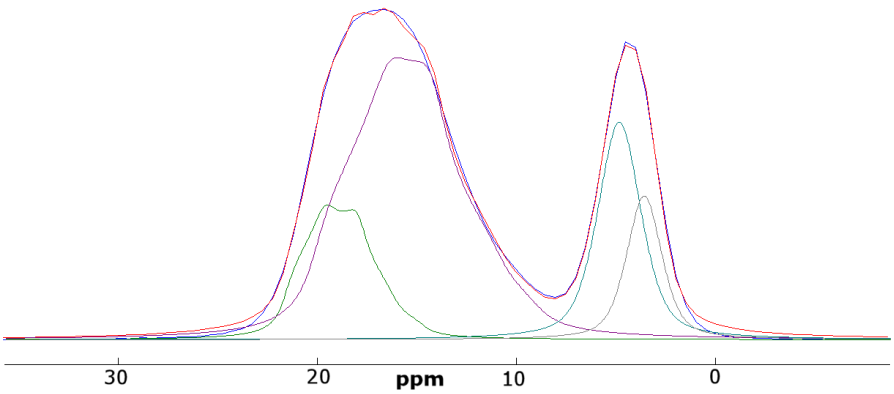

Figure 9. MAS NMR spectrum of $20Li_2O•80B_2O_3$ peak fitted in DMFit.

The peak areas were then given by the fitting program. The B3 area was multiplied by 1.04 to account for area lost to the spinning sidebands. It has been shown that the B4 area does not suffer from this effect and thus no adjustment is necessary [25].

The recorded signal was a whole echo centred in the middle of t_2 acquisition time. Exponential apodization of 250 Hz was applied to the centre of the 1st dimension. The 1st dimension was then complex Fourier transformed with a length equal number of acquisition points. It is important that the peak signal is the centre of the Fourier transform to enable accurate phasing. Next, the imaginary part of the spectrum was phased to zero signal, leaving the real part purely absorptive. The 2nd dimension was then Fourier transformed and reversed. This processed spectrum had every other point negative, as is expected in whole echo acquisition, and so the final processing was achieved by running a personally written macro to invert alternate points across the whole 2D frequency-domain spectrum, still within Spinsight.

III.3 Raman Experimental Details

All Raman spectra, from x=0 to x=40, were recorded by Ben Parkinson (University of Warwick postgraduate) using a Renishaw inVia Raman microscope running WiRE 2.0 software. The laser had a 514 nm wavelength and 10 mW power. The spectral width was 100 cm^{-1} to 3200 cm^{-1}. Each spectrum consisted of 50 acquisitions to improve the signal-to-noise ratio and the sampling region was at 50x magnification.

The laser beam was focused on to the surface of each sample, which was unpolished. Due to the varying thickness and roughness of the samples the absolute intensities of the spectra are not quantitatively comparable. However, as Raman spectroscopy is not a directly quantitative technique it is only the relative areas of the peaks that are of interest anyway.

The raw spectrum for each sample was imported into Origin 7.0 software for baseline subtraction. By picking several points that were assumed to represent a true zero at around 300 cm^{-1}, 1180 cm^{-1}, and then from 1700 cm^{-1} to 2000 cm^{-1}, a second order polynomial line could be fitted. The equation of this line was then entered as a baseline and subtracted from the data. This method was carried out identically for all samples except x=33 1/3 to x=40 which omitted the 1700 cm^{-1} data points.

Peak fitting of this baseline-subtracted data was also performed in Origin 7.0, after it was found that DMFit incorrectly renders the abscissa thus distorting relative peak areas. Each spectrum was assumed to have ten Gaussian peaks.

IV.1 Glass Creation Results

Compositions x=0 to x=35 were made from method 1. The pure B_2O_3 formed a toffee coloured lump~~blob~~, x=5 to x=25 formed lump~~blob~~s of transparent yellow glass and x=30 to x=35 crystallised.

Method 2 made compositions x=0 to x=40. Compositions x=0 to x=25 formed clear glass but there was still some devitrification for x=30 to x=40 and the sample yields were very low for the expected 20g product.

An observation of the inside of the furnace around 500°C during the ramping phase of method 2 showed the melts to be very frothy, overflowing the crucibles and touching each other as well as the furnace walls and heating elements. As the crucibles were only a quarter full of powder initially, this overflowing is most likely due to the rapid release of CO_2. Consequently these samples may be suffering from contamination and due to the mixing, be of altered composition.

Method 3 made compositions x=35 and x=40. Although the yields were larger for this run and despite the plate quenching, there was still portions of crystal mixed in with the glass. Throughout the rest of the report x=35 and x=40 will refer to these third method samples and the other compositions will refer to the second method samples.

The cobalt oxide glasses were also made with method 3. Mass measurements of the crucibles before and after the melt indicated mass losses of 3-4% from the expected 20 grams, thus they are expected to be suitably close to their desired nominal compositions. The cobalt oxide made the glasses appear a transparent pale blue for 0.1% CoO, to an intense blue that strongly absorbed light for 5% CoO. UV-Visible photospectrometry revealed the glasses strongly absorbed (>70% absorption) light between 500 nm and 650 nm.

X-ray diffraction (XRD) was performed on a selection of the lithium borate only samples to ensure they were glasses. A Hilton-Brooks XRD machine was used with a 40kV accelerating voltage and 30mA current striking a copper target tube. The 2θ angle was varied from 10° to 70° and over this range the spectrum was broad and featureless indicating a lack of long range order.

Scanning electron microscopy (SEM) was used to observe the surface of the x=40 sample at an interface between the transparent glass and small devitrified part. The surface had a thin layer of gold atoms sputtered onto it to make it conductive. Although the interface is discernible in visible light, to a 20kV electron beam both glassy and crystalline parts appeared similar due to their similar composition. At higher magnifications microscopic cracks were visible on the surface, probably caused by internal stress release due to the rapid cooling. Also visible on the surface were small regions of crystalline deposits that stood out as being of a different composition to the bulk material. Using energy dispersive X-ray analysis (EDX) on the bulk sample and these deposits it suspected they are KCl and NaCl crystals caused by handling.

Simultaneous thermal analysis (STA) was performed on samples x=30 to x=40 to determine their glass transition temperature (T_g) which reduces their compositional uncertainty. Ideally all samples would have been tested. The 20 mg samples were heated in small platinum crucibles along with quartz, a reference material, using a Perkin Elmer Pyris Diamond Thermogravimetric and Differential Thermal Analyzer under normal atmosphere.

x	Measured T_g (°C)	Implied x
30		
33 1/3		
35		
40		

Table 3. Measured glass transition temperatures, taken from the onset of the T_g peak, and implied composition from T_g value given in the literature [24].

Magnetic susceptibility measurements were made on the cobalt oxide glasses, cooled down to 50 (±0.5) °K, by measuring the magnetisation, *M*, as an applied magnetic field, *H*, was varied from 0 to 1 Tesla at a rate of 0.5 Tesla a minute. The relation:

$$M = \chi H \tag{8}$$

was used to find the magnetic susceptibility, χ.

Cobalt oxide (mol%)	χ (emu/g)	χ_ρ (m^3/kg)
0.2	0.010049	0.000126
0.5	0.041050	0.000516
1	0.088296	0.001110
2	0.172525	0.002168
5	0.385174	0.004840

Table 4. Magnetic susceptibility measurement results on cobalt oxide glass.

This increase in magnetic susceptibility has a clear effect on the NMR spectra of the cobalt glasses.

IV.2 NMR Spectroscopy Results

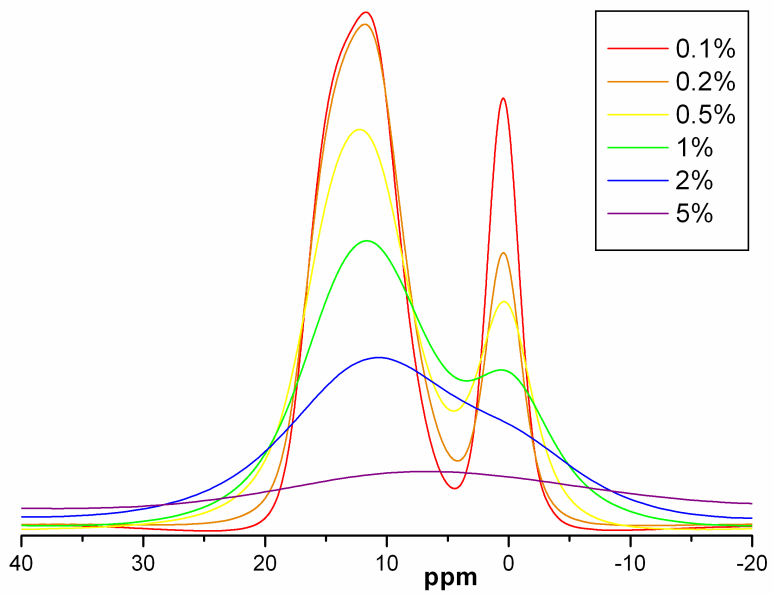

Figure 10. Boron-11 MAS NMR spectra showing the effect of increasing cobalt oxide (legend in mol%). Recorded using identical settings for all spectra. There is negligible sample quantity variation.

Figure 10 shows the effect of increasing magnetic susceptibility, caused in this case by the paramagnetic species, Co^{2+}. After 2 mol% CoO the B3/B4 peaks cannot be resolved and so an accurate N4 value is unfeasible using NMR.

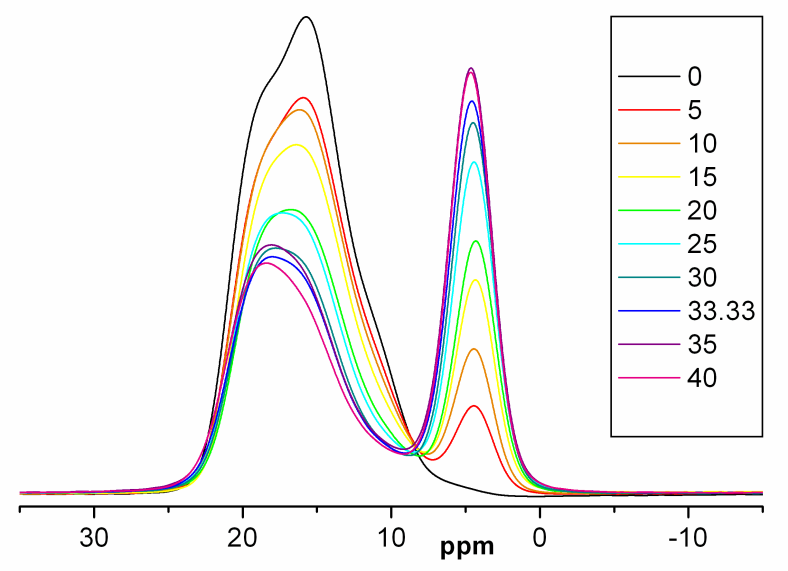

Figure 11. Boron-11 MAS NMR spectra, recorded using identical settings for all spectra. The legend refers to x in of $x\mathrm{Li_2O}\bullet(100\text{-}x)\mathrm{B_2O_3}$.

Figure 11 shows … B3/B4, trends, quadrupole fitting parameters:

x	Cq (k~~K~~Hz)	η
0	101.27	0.50
	136.69	0.67
5	106.81	0.57
	138.81	0.64
10	106.82	0.59
	138.58	0.62

x	Cq (k~~K~~Hz)	η
15	105.05	0.63
	137.59	0.60
20	104.56	0.50
	130.86	0.60
25	103.82	0.69
	135.82	0.55

x	Cq (k~~K~~Hz)	η
30	104.03	0.68
	134.99	0.55
35	104.69	0.49
	128.39	0.59
40	105.38	0.63
	135.55	0.57

Table 5. Quadrupole parameters for B3 peaks as given by DMFit.

Since performing the 3QMAS experiment it transpired that the CMX 4 mm probe lacked the power to suitably excite the triple-quantum coherence required by the experiment, hence the poor signal-to-noise ratio. [2D spectrum showing where the peaks *should* be]. Also, tests on rubidium nitrate ($\mathrm{RbNO_3}$) have revealed a departure from the expected spectrum in terms of shearing, bringing into question to accuracy of the specific pulse sequence used.

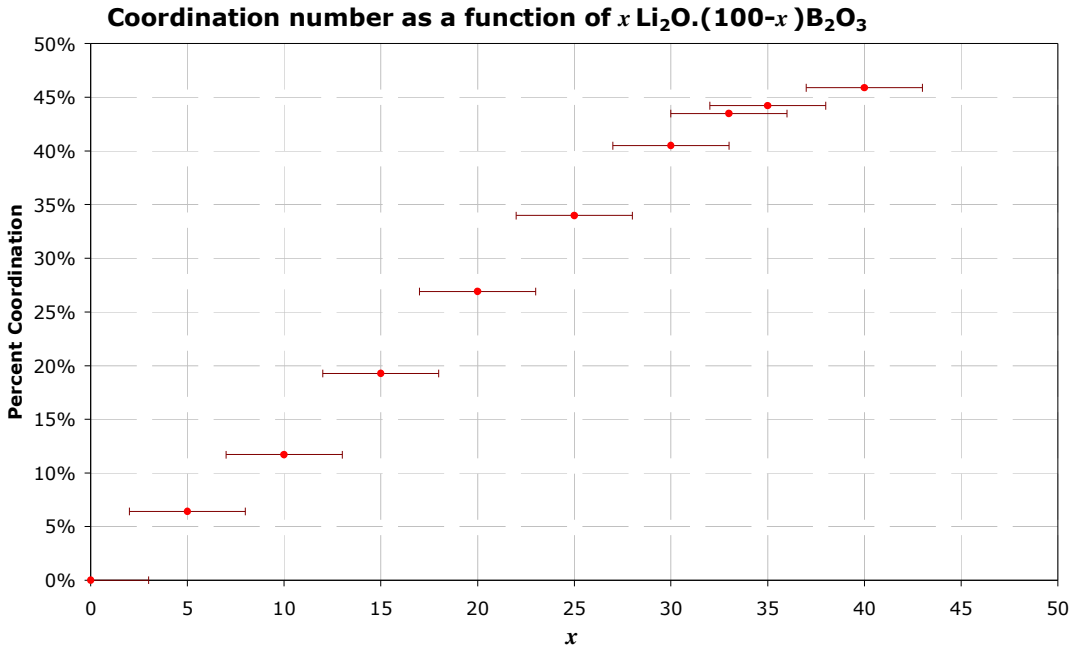

Not final graph – abscissa error bars need adjusting based on STA measurements and ordinate errors need adding

IV.3 Raman Spectroscopy Results

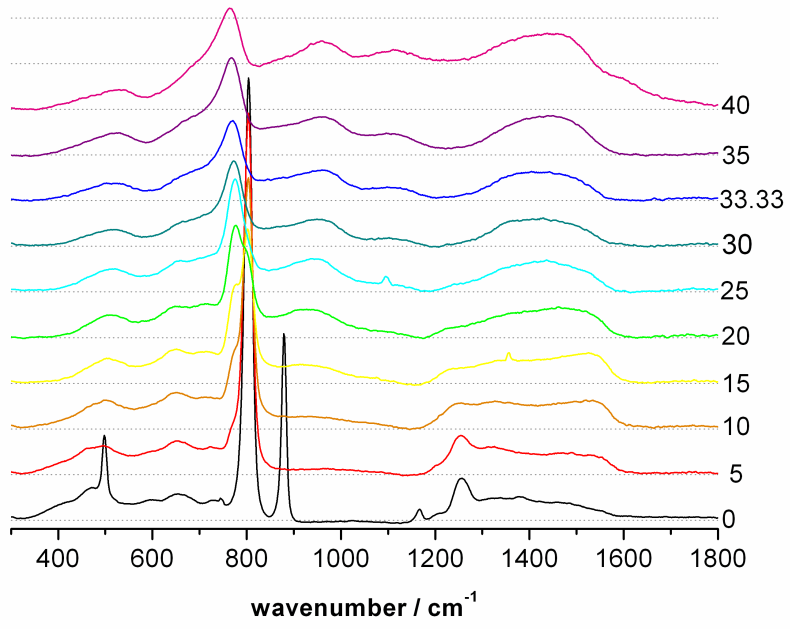

Not final graph – too much peak overlay!

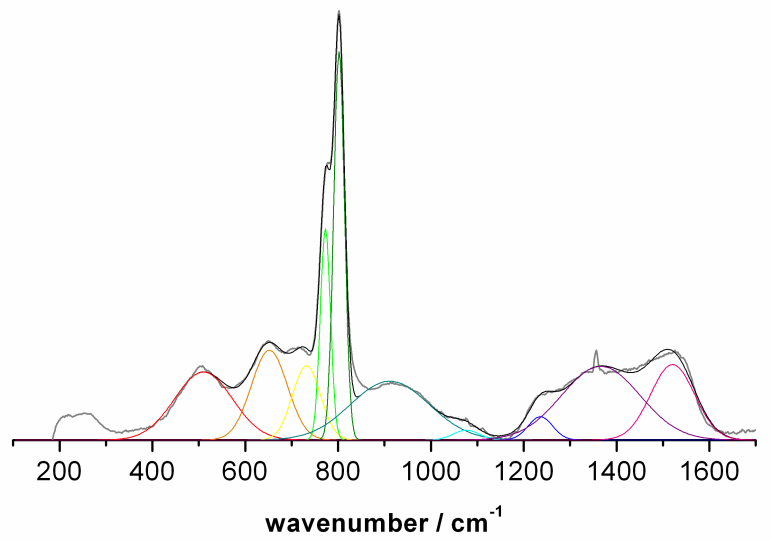

Not final graph – needs a title!

Peak assignments & N4 fraction from Raman data graph → peak assignments still in progress.

V. NMR – Raman Calibration

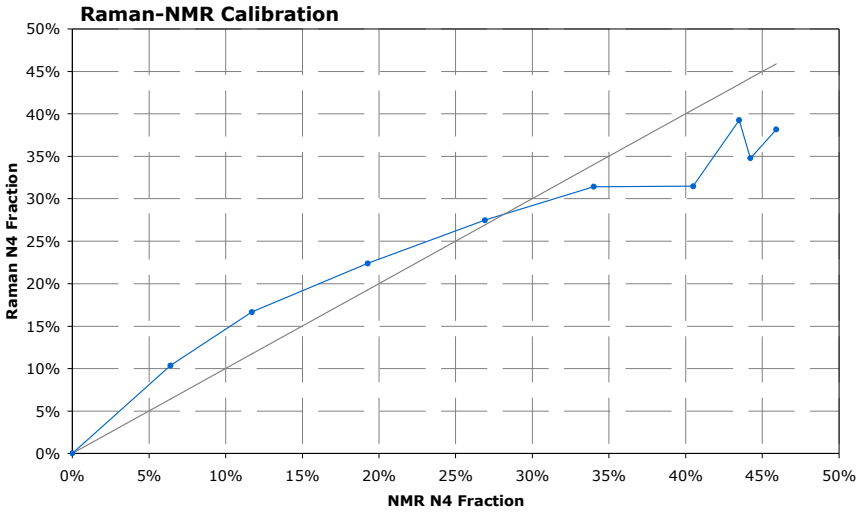

Not final graph – I haven't properly tweaked the superstructural unit assignments.

VI. Discussion

To Be Written.

Word count so far: ~6000

VII. Conclusions

To Be Written.

VIII. ACKNOWLEDGMENTS

Dr Diane Holland, Professor Ray Dupree, Professor Steve Feller for discussions on lithium borate glasses, Mr Ben Parkinson for Raman and STA measurements, Dr Ivan Hung for assistance with the MQMAS NMR technique, Dr Martin Lees for magnetisation measurements, Mr Keith Briggs for laboratory assistance, and Miss Jane Douglas.

IX. REFERENCES

[1] A. C. Wright, N. M. Vedishcheva & B. A. Shakhmatkin, *Mat. Res. Soc. Symp. Proc.*, 1997, **455**, 381-396

[2] B. N. Meera & J. Ramakrishna, *J. Non-Cryst. Solids*, 1993, **159**, 1-21

[3] B. P. Dwivedi, M. H. Rahman, Y. Kumar & B. N. Khanna, *J. Phys. Chems. Solids*, 1993, **54**, 621-628

[4] G. E. Jellison, S. A. Feller & P. J. Bray, *Phys. Chem. Glasses*, 1978, **19**, 52

[5] W. L. Konijnendijk & J. M. Stevels, *J. Non-Cryst. Solids*, 1975, **18**, 307-331

[6] E. I. Kamitsos, M. A. Karakassides & G. D. Chryssikos, *Phys. Chem. Glasses*, 1989, **30**, 229-234

[7] M. Royle, M. Sharma, S. Feller, J. MacKenzie & S. Nijhawan, *Phys. Chem. Glasses*, 1993, **34**, 149-152

[8] J. L. Shaw, A. C. Wright, R. N. Sinclair, J. R. Frueh, R. B. Williams, N. D. Nelson, M. Affatigato, S. A. Feller & C. R. Scales, *Phys. Chem. Glasses*, 2003, **44**, 256-259

[9] M. Massot, S. Souto & M. Balkanski, *J. Non-Cryst. Solids*, 1995, **182**, 49-58

[10] L. van Wüllen & W. Müller-Warmuth, *S. S. Nuc. Mag. Res.*, 1993, **2**, 279-284

[11] J. P. Amoureux, C. Fernandez & L. Frydman, *Chem. Phys. Lett.*, 1996, **259**, 347-355

[12] S-J. Hwang, C. Femandez, J. P. Amoureux, J. Cho, S. W. Martin & M. Pruski, *S. S. Nuc. Mag. Res.*, 1997, **8**, 109-121

[13] S. P. Brown & S. Wimperis, *J. Mag. Res.*, 1997, **124**, 279-286

[14] J. F. Stebbins, P. Zhao & S. Kroeker, *S. S. Nuc. Mag. Res.*, 2000, **16**, 9-19

[15] S. Kroeker, S. A. Feller, M. Affatigato, C. P. O'Brien, W. J. Clarida & M. Kodama, *Phys. Chem. Glasses*, 2003, **44**, 54-58

[16] W. J. Clarida, J. R. Berryman, M. Affatigato, S. A. Feller, S. C. Kroeker, J. Ash, J. W. Zwanziger, B. Meyer, F. Borsa & S. W. Martin, *Phys. Chem. Glasses*, 2003, **44**, 215-217

[17] L-S. Du & J. F. Stebbins, *J. Phys. Chem. B*, 2003, **107**, 10063-10076

[18] J. W. Zwanziger, *S. S. Nuc. Mag. Res.*, 2005, **27**, 5-9

[19] R. Kerner, *J. Non-Cryst. Solids*, 1991, **135**, 155-170

[20] A. Llor & J. Virlet, *Chem. Phys. Lett.*, 1988, **152**, 248-253

[21] http://www.kosi.com/Raman/resources/tutorial/, Raman Spectroscopy Tutorial by Kaiser Optical Systems, Inc.

[22] B. G. Parkinson, D. Holland, M. E. Smith, A. P. Howes & C. R. Scales, *J. Non-Cryst. Solids*, 2005, **351**, 2425-2432

[23] D. Massiot, F. Fayon, M. Capron, I. King, S. Le Calvé, B. Alonso, J-O. Durand, B. Bujoli, Z. Gan & G. Hoatson, *Magn. Res. Chem.*, 2002, **40**, 70-76

[24] M. Affatigato, S. Feller, E. J. Khaw, D. Feil, B. Teoh, & O. Mathew, *Phys. Chem. Glasses*, 1990, **31**, 19-24

[25] K. MacKenzie and M. E. Smith, *Multinuclear solid-state NMR of inorganic materials*, Pergamon Materials Series, 6, Pergamon-Elsevier, Oxford, 2002